Baryon production and collective flow in relativistic heavy-ion collisions in the AGS, SPS, RHIC, and LHC energy regions ($\sqrt{s_{NN}} \leqslant 5$ GeV to 5.5 TeV)

Shengqin Feng[1,2,3] and Yang Zhong[1]

[1]*College of Science, China Three Gorges University, Yichang 443002, China*

[2]*Key Laboratory of Quark and Lepton Physics (Huazhong Normal University), Ministry of Education, Wuhan 430079, China*

[3]*School of Physics and Technology, Wuhan University, Wuhan 430072, China*

(Received 12 November 2009; revised manuscript received 4 March 2011; published 24 March 2011)

The features of net-baryon productions and collective flow in relativistic heavy-ion collisions at energies reached at the CERN Large Hadron Collider (LHC), BNL Relativistic Heavy Ion Collider (RHIC), CERN Super Proton Synchrotron (SPS), and BNL Alternating Gradient Synchrotron (AGS) with the model of nonuniform flow model (NUFM) are systematically studied in this paper. In particular we predict the feature of net-baryon productions and collective flow at LHC $\sqrt{s_{NN}} = 5500$ GeV based on the detailed study at RHIC $\sqrt{s_{NN}} = 62.4$ and 200 GeV. The dependencies of the features of baryon stopping and collective flow on the collision energies and centralities are investigated.

DOI: 10.1103/PhysRevC.83.034908 PACS number(s): 25.75.Ld, 25.75.Dw

I. INTRODUCTION

Over the last two decades relativistic heavy-ion collisions [1,2] have been studied experimentally at increasingly higher center-of-mass energies at the Brookhaven Alternating Gradient Synchrotron (AGS) ($\sqrt{s_{NN}} < 5$ GeV), the CERN Super Proton Synchrotron (SPS) ($\sqrt{s_{NN}} \leqslant 20$ GeV), and the Brookhaven Relativistic Heavy Ion Collider (RHIC) ($\sqrt{s_{NN}} \leqslant 200$ GeV). As discussed in this article, the data collected in these experiments display remarkable generic trends as a function of system size and kinematic variables. The Large Hadron Collider (LHC) at CERN will study heavy-ion collisions at a center-of-mass energy $\sqrt{s_{NN}} = 5.5$ TeV, which is a factor of 27 higher than the maximum collision energy at RHIC. This is an even larger increase in center-of-mass energy than the factor of 10 going from the CERN SPS to BNL RHIC. It leads to a significant extension of the kinematic range in longitudinal rapidity and transverse momentum. The collectivity of high-energy density matter is one of the important properties in understanding high-energy heavy-ion collisions [3–5]. It is also challenging to understand how collectivity is generated during collisions.

There has been a lot of work in recent years on thermal and collective flow model calculations [6–18] of heavy-ion collisions to RHIC data and extrapolating them to the higher LHC energies. Here we should mention some kinds of models of thermal and collective flow. The first one is the spherically expanding source model that may be expected to approximate the fireball of an isotropic thermal distribution created in lower energy collisions.

As the collision energy increases, stronger longitudinal flow is formed which leads to a cylindrical geometry according to the second-kind model [16,17]. It accounts for the anisotropy of longitudinal and transverse direction by adding the contribution from a set of fireballs with centers located uniformly in the rapidity region of the longitudinal direction. It can account for the wider rapidity distribution at AGS and SPS when compared to the prediction of the pure thermal isotropic model.

Bjorken [18] postulated that the rapidity distribution of produced particles establishes a plateau at midrapidity which has been formulated for asymptotically high energies. It is well known that collisions at available heavy-ion energy regions of AGS, SPS, and RHIC are neither fully stopped nor fully transparent [19–27], although a significant degree of transparency is observed. But the central plateau structure becomes more and more obvious as the collision energy increases to SPS and RHIC.

As the collision energy increases to LHC, which is a factor 27 higher than the maximal collision energy at RHIC, the kinematic range in the longitudinal direction will increase considerably and the net-baryon density will decrease quickly at midrapidity. It seems reasonable to realize that the plateau proposed by Bjorken [18] at midrapidity at the LHC energy region has been established. For the net-baryon distributions, Ref. [28] realized that the collision of high-energy heavy ions can be divided into two different energy regions: the baryon-free quark gluon plasma (QGP) region (or the pure QGP region) with $\sqrt{s} > 100$ GeV per nucleon, and the baryon-rich QGP region (or the "stopping" region) with $\sqrt{s} \sim 5-10$ GeV per nucleon, which corresponds to about many tens of GeV per projectile nucleon in the laboratory system. In the baryon-free QGP region we need to know the nuclear stopping power to determine whether the beam baryons and the target baryons will recede away from the center-of-mass without being completely stopped, leaving behind QGP with very little baryon content.

The NUFM (nonuniform flow model) [29–34] realized that the fireballs keep some memory on the motion of the incident nuclei, and therefore the distribution of fireballs, instead of being uniform in the longitudinal direction, is more concentrated in the motion direction of the incident nuclei, that is, more dense at large absolute value of rapidity. It will not only lead to anisotropy in longitudinal-transverse directions, but also render the fireballs (especially for those baryons) distributing nonuniformly in the longitudinal direction. NUFM [29–34] may analyze the central dip of baryon rapidity distribution by assuming that the centers of fireballs are distributed nonuniformly in the longitudinal phase space.

This paper is organized as follows. In Sec. II we give a brief review the nonuniform flow model in the longitudinal

direction. The comparison and analysis of baryon distribution of AGS, SPS, RHIC, and LHC with the results of the model are given in Sec. III. Section IV gives a summary and conclusions.

II. NONUNIFORM FLOW MODEL (NUFM)

The NUFM model we considered [29–34] contains three distinct assumptions.

(i) It is argued that the transparency or stopping of relativistic heavy-ion collisions should be taken into account more carefully. A more reasonable assumption is that the fireballs keep some memory on the motion of the incident nuclei, and therefore the distribution of fireballs, instead of being uniform in the longitudinal direction, is more concentrated in the direction of motion of the incident nuclei, that is, more dense at large absolute value of rapidity. It will not only lead to anisotropy in longitudinal-transverse directions, but also render the fireballs (especially for those baryons) distributing nonuniformly in the longitudinal direction.

(ii) The freeze-out temperatures are assumed to be about the same around 120 MeVwhether it is at higher LHC or at lower AGS energy region. Since the temperature at freeze out exceeds 100 MeV, the Boltzmann approximation seems reasonable to study LHC at freeze out.

(iii) In order to express the nonuniformity of flow in the longitudinal direction, an ellipticity parameter e is introduced through a geometrical parametrization. For the central collisions the nuclear stopping can be studied by the range of rapidity of emission source in the center-of-mass system.

We have previously used NUFM to study the net proton rapidity among AGS, SPS, and RHIC energy regions [30]. But for the RHIC energy regions we made an earlier error [30] to predict the distributions of net proton distributions since we neglected the effects of the baryon number conservation. Therefore, it is necessary to reanalyze the features of net proton rapidity distributions among AGS to RHIC by taking into account the baryon number conservation. It is found that when we consider the baryon number conservation, the features of the distributions at RHIC are completely different from the results given before [30], especially in the large absolute rapidity region. On the other hand, with the run of forthcoming LHC the predictions of the features of net proton rapidity distributions at LHC are also important. We will restudy the features of net proton rapidity distributions among AGS to RHIC by using NUFM, and make prediction for the features of forthcoming LHC in this paper. In the following we will first make a simple introduction to the NUFM.

A parametrization for such a nonuniform distribution can be obtained by using an ellipse-like picture on emission angle distribution. In this scenario the emission angle is

$$\theta = \tan^{-1}(e \tan \Theta). \tag{1}$$

Here the induced parameter $e\,(0 \leqslant e \leqslant 1)$ represents the ellipticity of the introduced ellipse which describes the nonuniform of fireball distribution in the longitudinal distribution. The detailed discussions of the NUFM were given by Ref. [29]. The rapidity distribution of NUFM is

$$\frac{dn_{\mathrm{NUFM}}}{dy} = eKm^2T \int_{-y_{e0}}^{y_{e0}} \rho(y_e) dy_e (1 + 2\Gamma + 2\Gamma^2) e^{-1/\Gamma}, \tag{2}$$

y_{e0} and e are the important parameters in this paper, y_{e0} is the rapidity limit which confines the rapidity interval of longitudinal flow, and e can describe the nonuniform in the longitudinal direction of the collective flow. In Eq. (2),

$$\Gamma = \frac{T}{m \cosh(y - y_e)}, \tag{3}$$

m is the mass of produced particle, T is the temperature parameter, y_e is the rapidity of collective flow,

$$\rho(y_e) = \sqrt{\frac{1 + \sinh^2(y_e)}{1 + e^2 \sinh^2(y_e)}} \tag{4}$$

is the flow distribution function in the longitudinal direction, and e is a parameter which represents the ellipticity of the introduced ellipse describing the nonuniform of fireball distribution in the longitudinal direction. It may be figured out from Eq. (2) to Eq. (4) that the larger the parameter e, the flatter the distribution function $\rho(y_e)$, the more uniform the longitudinal flow distribution. When $e \Rightarrow 1$ the longitudinal flow distribution is completely uniform $\rho(y_e) \Rightarrow 1$ and returns to uniform flow. The other important parameter y_{e0} describes the kinematic region and can determine the width of the distribution.

In order to discuss the dependence of velocity of collective flow on collision energy in the central mass (CM) system, we give a calculation of the average velocity in the longitudinal direction as $\langle \beta_L \rangle = \tanh(y_{e0}/2)$ and $\langle \beta\gamma \rangle_L$, where $\gamma = 1/\sqrt{1 - \langle \beta_L \rangle^2}$ is the Lorentz factor. Therefore y_{e0} can also determine the average velocity of collective flow in the longitudinal direction.

III. THE NET PROTON DISTRIBUTIONS AT THE WHOLE AGS TO LHC ENERGY REGIONS

We use the form of the NUFM model as described in Sec. II and fit the experimental data with the parameters y_{e0} and e that have been assumed to be different for different energies (as given in Table I). The systematics of these parameters provide useful information on the collective flow of baryons in these reactions.

Comparing with NUFM calculation before [30], we consider the influence of baryon number conservation when discussing the distributions. Figure 1(a) shows net-proton rapidity distributions measured at AGS and SPS energies. Figure 1(b) shows net-proton rapidity distributions of the top 5% central collisions measured at RHIC $\sqrt{s_{NN}} = 62.4$ and $\sqrt{s_{NN}} = 200$ GeV, respectively. The solid lines are our NUFM calculation results from AGS to RHIC and the dotted line is the calculation result for that of LHC. It can be seen from Fig. 1 that NUFM model can fit the experimental results from AGS to RHIC and reproduce the central dip of the rapidity distribution of the proton at SPS and RHIC in agreement with the experimental findings. y_{e0} is approximately equal to the half width of fit

TABLE I. The different parameters of net-proton distribution by using NUFM from AGS to LHC.

$E_{\rm lab}$ or $\sqrt{s_{NN}}$ (GeV)	y_p	$\langle\delta_y\rangle$	$\langle\beta\gamma\rangle_{\rm L}$	e	y_{e0}
$E_{\rm lab} = 2$ (Au + AuA GS)	0.6951	0.3519	0.3255	1.0	0.648
$E_{\rm lab} = 4$ (Au + Au AGS)	1.0647	0.5391	0.4653	1.0	0.910
$E_{\rm lab} = 6$ (Au + Au AGS)	1.2714	0.6332	0.5897	1.0	1.124
$E_{\rm lab} = 8$ (Au + Au AGS)	1.4166	0.6997	0.6189	1.0	1.168
$E_{\rm lab} = 10.8$ (Au + Au AGS)	1.5674	0.9499	0.6967	0.82	1.300
$E_{\rm lab} = 14.6$ (Si + Al AGS)	1.7186	0.7989	0.7256	0.72	1.684
$E_{\rm lab} = 158$ (Pb + Pb SPS)	2.9112	1.6774	1.4558	0.61	2.340
$E_{\rm lab} = 200$ (S + S SPS)	3.0283	1.1336	1.6542	0.554	2.960
$\sqrt{s_{NN}} = 62.4$ (Au + Au RHIC)	4.197	1.9528	3.2682	0.34	4.860
$\sqrt{s_{NN}} = 200$ (Au + Au RHIC)	5.36	2.3021	7.7894	0.31	5.320
$\sqrt{s_{NN}} = 5500$ (Pb + Pb LHC)	8.4669	3.5724	32.7912	0.19	7.880

distribution. In a sense the parameter y_{e0} represent the kinetic region of collective flow in the longitudinal direction. The parameter of T is chosen to be 0.12 GeV.

The features of nonuniform flow distributions show strong energy dependence from AGS to RHIC. For example, at AGS ($e = 0.82$, $E_{\rm lab} = 10.8$ GeV) the net proton distribution has a peak at midrapidity and the distribution is narrower than that of the other two energies. The collective flow is approximately uniform. While at SPS ($e = 0.61$) a dip begins to show in the middle of rapidity distribution. While at RHIC $\sqrt{s_{NN}} = 62.4$ GeV and $\sqrt{s_{NN}} = 200$ GeV the distributions show deep dip and the nonuniform parameter e takes 0.34 and 0.31, respectively. According to our calculation as the collision energy increases the net-baryon distributions become wide for the whole rapidity distribution and the net-baryon densities become small at the middle rapidity ($y \approx 0$) region.

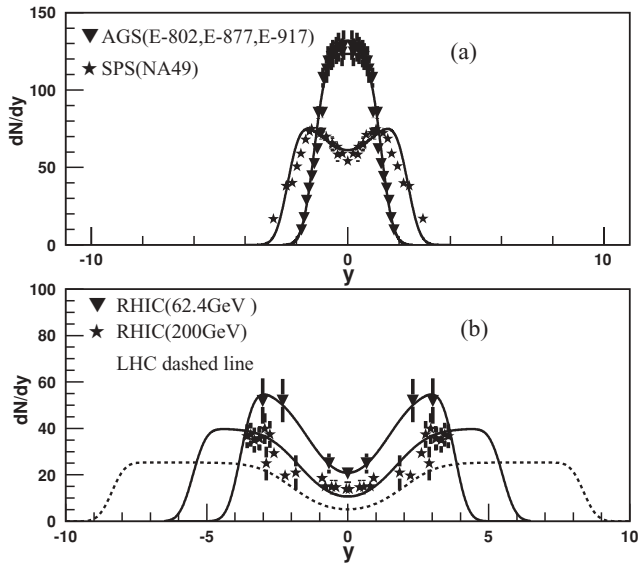

FIG. 1. The net proton distribution at AGS and SPS are shown in (a). The net proton distribution at RHIC $\sqrt{s_{NN}} = 62.4$ GeV and $\sqrt{s_{NN}} = 200$ GeV are shown in (b). The experimental results come from [19–27], the dotted line which is predicted by NUFM for LHC is shown in (b).

We also speculate on the feature of nonuniform flow distributions at LHC in Fig. 1(b). As mentioned before, although collisions at available heavy-ion energy regions of AGS, SPS, and RHIC are neither fully stopped nor fully transparent, the plateau structure becomes more and more obvious as the collision energy increases to SPS and RHIC. It leads to a significant extension of the kinematic range (y_{e0}) in longitudinal rapidity and the net-baryon distribution at the central rapidity region decreases at LHC. It seems reasonable that the kinematic range (y_{e0}) at LHC $\sqrt{s_{NN}} = 5500$ GeV approaches the incident beam rapidity y_p, which is about 1.5 times that at RHIC $\sqrt{s_{NN}} = 200$ GeV ($y_{e0} = 5.32$).

By making a analysis of the dependence of $dN/dy|_{y=0}$ on incident beam rapidity y_p from SPS ($\sqrt{s_{NN}} = 17.2$ GeV) to RHIC ($\sqrt{s_{NN}} = 62.4$ and 200 GeV) experiments, in which the rapidity distribution obviously shows central dip feature, we can provide a relationship between $dN/dy|_{y=0}$ and incident beam rapidity y_p,

$$dN/dy|_{y=0} = 51.0 - 22.0 \cdot \log(y_p) \tag{5}$$

shown in Fig. 2. According to the speculation the magnitude of rapidity density at central rapidity $y \approx 0$ at LHC is about 3.63 which is about 1/4 times that at RHIC 200 GeV. We can get $e = 0.19$ to fit the LHC distribution by using the NUFM and the baryon number conservation law.

At LHC a broad dip in the middle of rapidity region has developed spanning several units of rapidity, indicating that collisions are quite transparent at the LHC energy region. According to our study $e = 0.19$ at LHC gives a more obvious nonuniform feature than that of AGS, SPS, and RHIC energy region, and the detailed results are shown in Table I.

From Fig. 3 we know that as the incident energy increases the longitudinal flow distribution becomes more nonuniform. $e = 0.19$ at LHC $\sqrt{s_{NN}} = 5500$ GeV is smaller than $e = 0.31$ at RHIC $\sqrt{s_{NN}} = 200$ GeV, and $e = 0.82$ at AGS ($E_{\rm lab} = 10.8$ GeV). The central rapidity density at AGS is the largest in the whole AGS, SPS, RHIC, and LHC energy regions in Fig. 3.

Figure 4 shows proton rapidity distribution at different collision energies at AGS and SPS, and the solid lines are the calculation results. From Fig. 4 we know that proton distribution shows uniform distribution feature in the longitudinal direction at the AGS (2–8 GeV) according to NUFM.

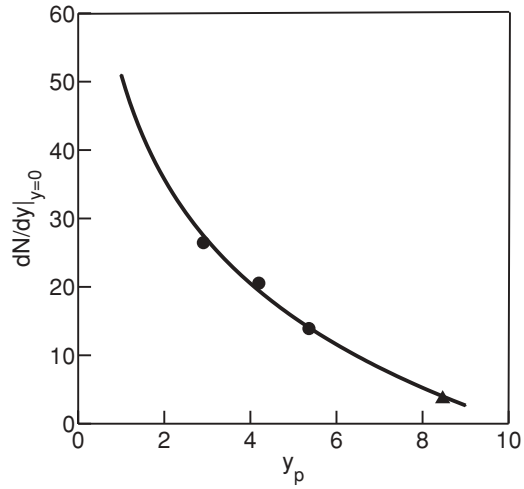

FIG. 2. The dependence of central rapidity density $dN/dy|_{y=0}$ on incident beam rapidity y_p from SPS ($\sqrt{s_{NN}} = 17.2$ GeV) to RHIC ($\sqrt{s_{NN}} = 62.4$ and 200 GeV) experiments. The solid circles are from experimental results and the solid triangle is the speculating result at LHC. The real line is the fit curve of Eq. (5).

But for Pb + Pb interactions (158 GeV) at SPS $e = 0.61$ shows a nonuniform distribution feature in the longitudinal direction.

Figure 5 shows proton distribution at different collision systems AGS and SPS. It is found from Fig. 5 that $e = 1$ and $y_{e0} = 1.411$ for heavier collision system (Au + Au), but $e = 0.72$ and $y_{e0} = 1.609$ for lighter collision system (Si + Al) at AGS. It is suggested that the lighter the collision system the more nonuniform the distribution in the longitudinal direction and the larger the kinematical limitation. The same situation is shown at SPS compared with AGS.

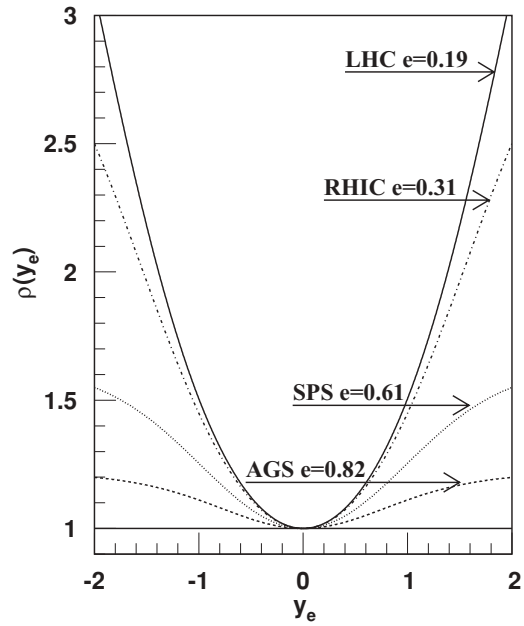

FIG. 3. The flow distribution function of net proton in the longitudinal direction in the whole AGS, SPS, RHIC, and LHC energy regions.

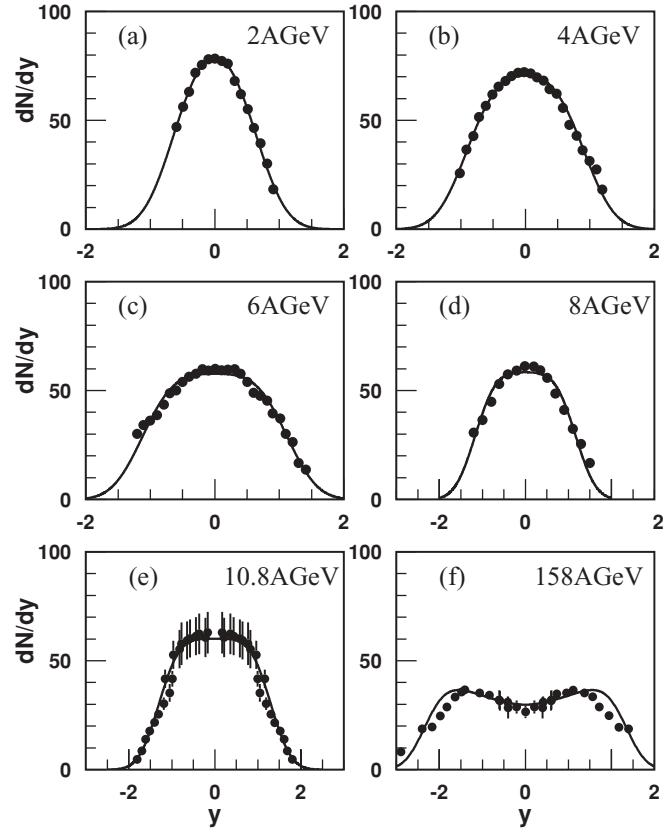

FIG. 4. Proton rapidity distributions for Au + Au interaction at AGS. The experimental data is from Refs. [22–27] and the solid lines are the calculation results. The whole fitted parameters e and quanta y_{e0} are given in Table I.

From the calculation we find that y_{e0} determines the width of distribution and confines the flow kinetics regions $\langle \beta\gamma \rangle_L$.

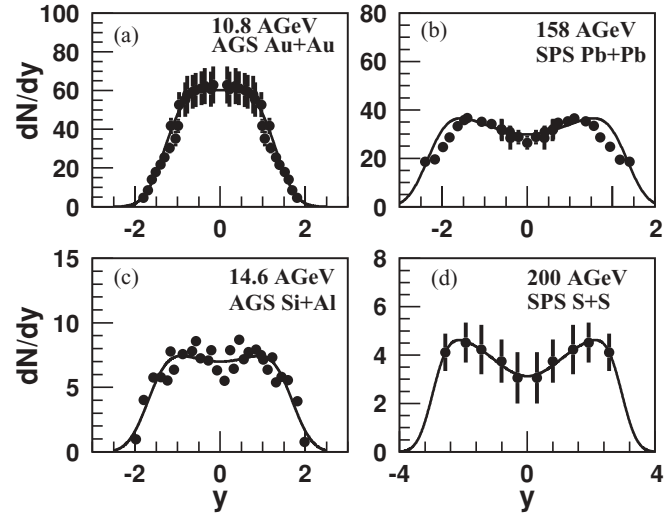

FIG. 5. Proton rapidity distributions for Au + Au (10.8 GeV) and Si + Al (14.6 GeV) interactions at AGS, and for Pb + Pb (158 GeV) and S + S (200 GeV) interactions at SPS. The experimental data are from Refs. [22–27] and the solid lines are the calculation results. The whole fitted parameters e and quanta y_{e0} are given in Table I.

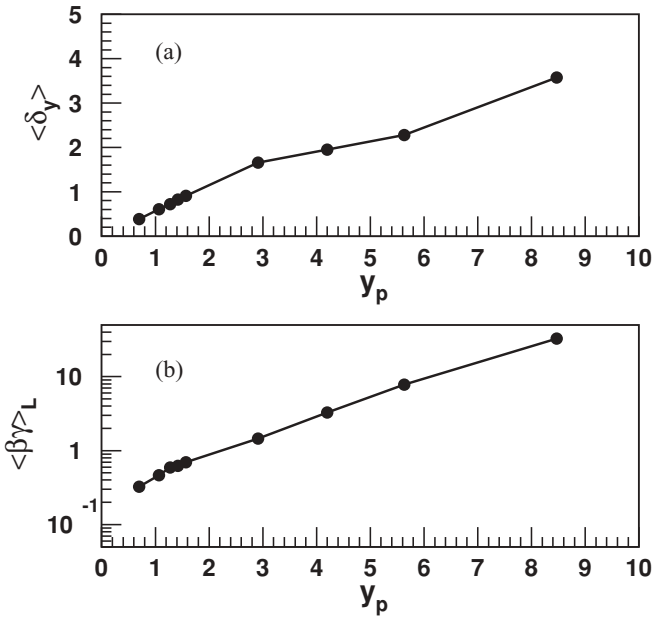

FIG. 6. The dependence of average rapidity loss $\langle \delta y \rangle$ (a) and $\langle \beta\gamma \rangle_L$ (b) on incident proton rapidity in the whole AGS, SPS, RHIC, and LHC energy regions.

It is found that the depth of the central dip of the net-baryon distributions depends on the magnitude of the parameter e that describes the nonuniformity of longitudinal flow.

The stopping may be estimated from the rapidity loss experienced by the baryons in the colliding nuclei. If incoming beam baryons have rapidity y_p relative to the CM, the average rapidity loss of net proton is

$$\langle \delta y \rangle = y_p - \langle y \rangle, \tag{6}$$

where $\langle y \rangle$ is the average rapidity of net proton:

$$\langle y \rangle = \frac{2}{N_{\text{part}}} \int_0^{y_p} y dy \frac{dN_{B-\bar{B}}(y)}{dy}, \tag{7}$$

where N_{part} is participant nucleon number. y_p is rapidity of incoming beam baryons relative to the CM. The $\langle y \rangle$ is given by

$$\langle y \rangle = \frac{\int_0^{y_p} y dy \frac{dn}{dy}}{\int_0^{y_p} dy \frac{dn}{dy}}, \tag{8}$$

where dn/dy is given by NUFM.

From Fig. 6(a) and Table I we know that from AGS to SPS average rapidity loss $\langle \delta y \rangle$ increases linearly with y_p. When discussing at RHIC we study the average rapidity loss at $\sqrt{s_{NN}} = 62.4$ and 200 GeV, a new linear increasing relationship is established from SPS to RHIC, but begins to increase slowly and deviates from that of AGS to SPS. We also predict the nuclear stopping power at LHC. The dependence of $\langle \beta\gamma \rangle_L$ (b) on incident proton rapidity in the whole AGS, SPS, RHIC, and LHC energy regions are shown in Fig. 6(b). We can find a kind of Log increasing dependence of $\langle \beta\gamma \rangle_L$ (b) on incident proton rapidity.

As shown in Fig. 7, NUFM can fit the net-baryon distribution at different centralities of 0%–10%, 10%–20%, 20%–40%, and 40%–60% at RHIC $\sqrt{s_{NN}} = 200$ GeV. From Fig. 8 and Table II we know that as the centrality increases the kinematic region and average velocity $\langle \beta\gamma_L \rangle$ in the longitudinal direction increases and the distribution becomes wide. On the other hand, the stopping power diminishes as the centrality increases. It is a surprise to find that the nonuniformity e keeps unchanged.

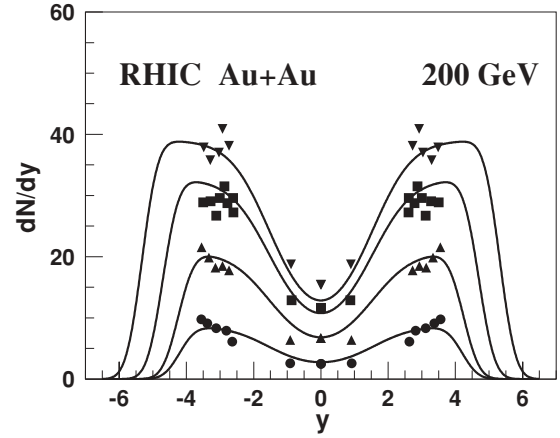

FIG. 7. Rapidity distribution of net baryons in Au + Au collisions at RHIC energy of $\sqrt{s_{NN}} = 200$ GeV are compared with preliminary BRAHMS net-baryon data [35] for different centralities of 0%–10%, 10%–20%, 20%–40%, and 40%–60%.

IV. SUMMARY AND CONCLUSION

Net-proton rapidity distributions have been measured by several experiments at different energies from AGS to RHIC. The compiled data are shown in Fig. 1. The net-proton rapidity distributions are reconstructed among the AGS, SPS, RHIC, and LHC energy regions by using NUFM in this work. We can predict the distribution feature in the fragmentation region of the net-proton distributions at RHIC although RHIC [19] only provided the multiplicity distribution of net protons at the central rapidity region. While at RHIC $\sqrt{s_{NN}} = 62.4$ GeV and $\sqrt{s_{NN}} = 200$ GeV the distributions show deep dip and the nonuniform parameter e takes 0.34 and 0.31, respectively. According to our calculation as the collision energy increases, the net-baryon distributions become wide for the whole rapidity distribution and the net-baryon densities become small at the middle rapidity ($y \approx 0$) region.

The features of nonuniform flow distributions show strong energy dependence from AGS to RHIC. For example, the net

TABLE II. The fit parameters of net-proton distribution for different centralities of 0%–10%, 10%–20%, 20%–40%, and 40%–60% by using NUFM at RHIC $\sqrt{s_{NN}} = 200$ GeV.

Centrality at $\sqrt{s_{NN}} = 200$ GeV	y_{e0}	$\langle \delta y \rangle$	$\langle \beta\gamma \rangle_L$	e
0%–10% (Au + Au RHIC)	5.320	2.318	7.113	0.31
10%–20% (Au + Au RHIC)	4.699	2.575	5.195	0.31
20%–40% (Au + Au RHIC)	4.239	2.822	4.106	0.31
40%–60%(Au + Au RHIC)	4.199	2.844	4.022	0.31

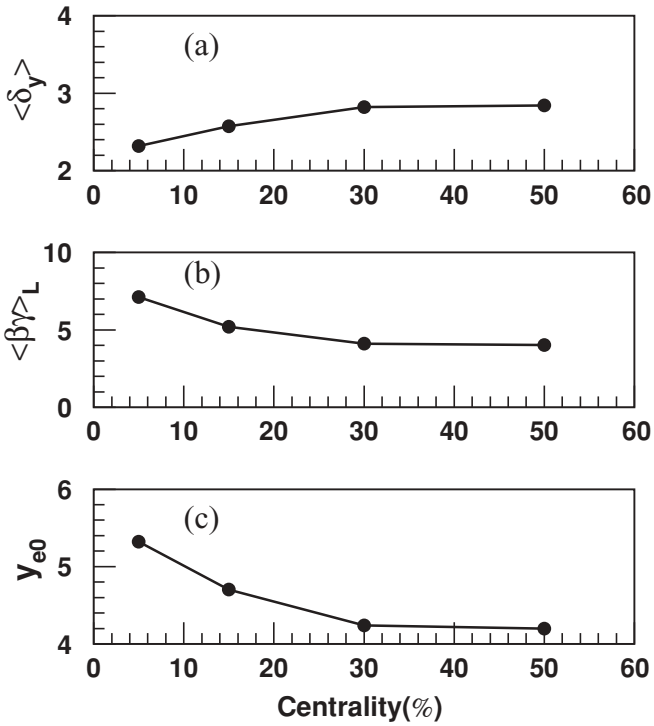

FIG. 8. The dependence of average rapidity loss $\langle \delta y \rangle$ (a), $\langle \beta\gamma \rangle_L$ (b), and kinematic region y_{e0} (c) on the collision centrality at RHIC $\sqrt{s_{NN}} = 200$ GeV.

proton distribution at AGS has a peak at midrapidity, and the distribution is narrower than that of the other two energies. The collective flow is approximately uniform. While at SPS a dip begins to show in the middle of rapidity distribution. The distributions at RHIC $\sqrt{s_{NN}} = 62.4$ GeV and $\sqrt{s_{NN}} =$ 200 GeV show the nonuniform feature of deep dip. It is found that the distributions become wider and wider for the whole rapidity distribution and the densities of net baryon in the middle of rapidity region ($y \approx 0$) become smaller and smaller.

Here we should mention that quite a few theoretical models [36–40] can give equally good representation of the data of particle productions in relativistic heavy ion collisions. These models give some different physical pictures for the research. In Ref. [38], in order to determine whether a pure quark-gluon plasma with no net-baryon density could be formed in the central rapidity region in relativistic heavy ion collisions, Wong [38] estimated the baryon distribution by using Glauber-type multiple collisions in which the nucleons of one nucleus degrade in energy as they make collisions with nucleons in the other nucleus. It was found that in the head-on collision of two heavy nuclei ($A \geqslant 100$) the baryon rapidity distributions have broad peaks and extend well.

The plateau structure becomes more and more obvious as the collision energy increases to RHIC although collisions at available heavy-ion energy regions of AGS, SPS, and RHIC are neither fully stopped nor fully transparent. It leads to a significant extension of the kinematic range (y_{e0}) in longitudinal rapidity and the net-baryon distribution at the central rapidity region decreases at LHC. We can study the feature of net-baryon distributions at LHC by using the NUFM and the baryon number conservation law.

Detailed energy dependence of the net-baryon distribution among AGS, SPS, and RHIC shows a clear transition from the baryon stopping region to the baryon transparent region. It is found that from AGS to SPS average rapidity loss $\langle \delta y \rangle$ increases linearly with y_p, but begins to increase slowly and deviates from the linear relationship when at RHIC and LHC. It may suggest the difference of the interaction mechanism in RHIC and LHC from AGS and SPS. The detailed study of net-proton rapidity distributions from AGS to LHC will deepen our study of the relativistic heavy-ion collisions.

It is found that the transparency of relativistic heavy-ion collisions increases as collision energy increases, that is, the higher the collision energy the more transparent the collision system by analyzing the proton rapidity distribution. The phase space of heavy collision system is nearly completely uniform in the longitudinal direction at AGS. The phase space of proton distributes nonuniformly in the longitudinal direction at SPS and RHIC. At LHC a broad dip in the middle of the rapidity region has developed spanning several units of rapidity, indicating that collisions are quite transparent at the LHC energy region. According to our study, $e = 0.19$ at LHC gives a more obvious nonuniform feature than that of AGS, SPS, and RHIC energy regions. By reanalyzing RHIC, we obtain a wider rapidity distribution than that of Ref. [30].

ACKNOWLEDGMENTS

This work was supported by the National Natural Science Foundation of China (10975091), Excellent Youth Foundation of Hubei Scientific Committee (2006ABB036), and Education Commission of Hubei Province of China (Z20081302). The authors are indebted to Professor Lianshou Liu for his valuable discussions and very helpful suggestions.

[1] A. H. Mueller, Nucl. Phys. B **572**, 227 (2000).
[2] P. Jacobs and X. N. Wang, Prog. Part. Nucl. Phys. **54**, 443 (2005).
[3] N. Armesto *et al.*, J. Phys. G **35**, 054001 (2008).
[4] F. Cooper and G. Frye, Phys. Rev. D **10**, 186 (1974).
[5] L. D. Landau, Izv. Akad. Nauk Ser. Fiz. **17**, 51 (1953).
[6] D. Teaney, J. Lauret, and E. V. Shuryak, Phys. Rev. Lett. **86**, 4783 (2001).
[7] T. Hirano, K. Morita, S. Muroya, and C. Nonaka, Phys. Rev. C **65**, 061902 (2002); K. Morita, S. Muroya, C. Nonaka, and T. Hirano, *ibid.* **66**, 054904 (2002).
[8] M. Gyulassy, P. Levai, and I. Vitev, Phys. Rev. Lett. **85**, 5535 (2000); Nucl. Phys. B **594**, 371 (2001).
[9] D. Kharzeev and M. Nardi, Phys. Lett. B **507**, 121 (2001).
[10] F. Becattini, J. Cleymans, A. Keranen, E. Suhonen, and K. Redlich, Phys. Rev. C **64**, 024901 (2001); J. Cleymans and K. Redlich, Phys. Rev. Lett. **81**, 5284 (1998).
[11] D. H. Rischke, S. Bernard, and J. A. Maruhn, Nucl. Phys. A **595**, 346 (1995); D. H. Rischke, Y. Pursun, and J. A. Maruhn, *ibid.* **595**, 383 (1995); **596**, 717(E) (1996).
[12] S. A. Bass *et al.*, Prog. Part. Nucl. Phys. **41**, 225 (1998).

[13] Y. M. Sinyukov, S. V. Akkelin, and Y. Hama, Phys. Rev. Lett. **89**, 052301 (2002); S. V. Akkelin, M. S. Borysova, and Yu. M. Sinyukov, Acta Phys. Hung. A **22**, 165 (2005).
[14] D. K. Srivastava, J. Alam, and B. Sinha, Phys. Lett. B **296**, 11 (1992); D. K. Srivastava, J. Alam, S. Chakrabarty, B. Sinha, and S. Raha, Ann. Phys. **228**, 104 (1993); D. K. Srivastava, J. Alam, S. Chakrabarty, S. Raha, and B. Sinha, Phys. Lett. B **278**, 225 (1992).
[15] P. F. Kolb, U. W. Heinz, P. V. Ruuskanen, and S. A. Voloshin, Phys. Lett. B **503**, 58 (2001); P. F. Kolb, P. Huovinen, U. W. Heinz, and H. Heiselberg, *ibid.* **500**, 232 (2001); P. F. Kolb, U. W. Heinz, P. Huovinen, K. J. Eskola, and K. Tuominen, Nucl. Phys. A **696**, 197 (2001).
[16] E. Schnedermann, J. Sollfrank, and U. Heinz, Phys. Rev. C **48**, 2462 (1993); U. Mayer and U. Heinz, *ibid.* **56**, 439 (1997); E. Schnedermann and U. Heinz, *ibid.* **50**, 1675 (1994); U. Heinz, Nucl. Phys. A **661**, 140c (1999).
[17] P. Braun-Munzinger, J. Stachel, J. P. Wessels, and N. Xu, Phys. Lett. B **365**, 1 (1996); **344**, 43 (1995); P. Braun-Munzinger and J. Stachel, Nucl. Phys. A **606**, 320 (1996).
[18] J. D. Bjorken, Phys. Rev. D **27**, 140 (1983).
[19] I. G. Bearden *et al.*, Phys. Rev. Lett. **93**, 102301 (2004).
[20] I. G. Bearden *et al.*, Phys. Rev. Lett. **94**, 162301 (2005).
[21] J. L. Klay *et al.*, Phys. Rev. Lett. **88**, 102301 (2002).
[22] L. Ahle *et al.*, Phys. Rev. C **60**, 064901 (1999).
[23] J. Barrette *et al.*, Phys. Rev. C **62**, 024901 (2000).
[24] H. Appelshauser *et al.*, Phys. Rev. Lett. **82**, 2471 (1999).
[25] F. Videbeck, Nucl. Phys. A **590**, 249 (1995).
[26] T. Wienold *et al.*, Nucl. Phys. A **610**, 76c (1996).
[27] B. B. Back *et al.*, Phys. Rev. Lett. **86**, 1970 (2001).
[28] C. Y. Wong, *Introduction to High-Energy Heavy-Ion Collisions* (World Scientific, Singapore, 1994).
[29] S. Q. Feng, F. Liu, and L. S. Liu, Phys. Rev. C **63**, 014901 (2000).
[30] S. Q. Feng, X. B. Yuan, and Y. F. Shi, Mod. Phys. Lett. A **21**, 663 (2006).
[31] S. Q. Feng and W. Xiong, Phys. Rev. C **77**, 044906 (2008).
[32] S. Q. Feng and X. B. Yuan, Sci. China Ser. G **52**, 198 (2009).
[33] X. Cai, S. Q. Feng, Y. D. Li, C. B. Yang, and D. C. Zhou, Phys. Rev. C **51**, 3336 (1995).
[34] S. Q. Feng, *Introduction to Multi-hadron Productions at High Energy Heavy-Ion Collisions* (Beijing Institute of Technology Press, Beijing, 2005) (in Chinese).
[35] R. Debbe *et al.*, J. Phys. G **35**, 104004 (2008).
[36] L. P. Csernai and J. I. Kapusta, Phys. Rev. D **31**, 2795 (1985).
[37] C. Y. Wong, Phys. Rev. Lett. **52**, 1393 (1984).
[38] C. Y. Wong, Phys. Rev. D **30**, 972 (1984).
[39] R. C. Hwa, Phys. Rev. Lett. **52**, 492 (1984).
[40] S. Jeon and J. Kapusta, Phys. Rev. C **56**, 468 (1997).